J Biol Inorg Chem (2005) 10: 946–957
DOI 10.1007/s00775-005-0047-8

ORIGINAL ARTICLE

Susanna Herold · Alain Puppo

Kinetics and mechanistic studies of the reactions of metleghemoglobin, ferrylleghemoglobin, and nitrosylleghemoglobin with reactive nitrogen species

Received: 21 June 2005 / Accepted: 3 October 2005 / Published online: 3 November 2005

Abstract It is now established that nitrogen monoxide is produced not only in animals but also in plants. However, much less is known about the pathways of generation and the functions of $NO^{\bullet}$ *in planta*. One of the possible targets of $NO^{\bullet}$ is leghemoglobin (Lb), the hemoprotein found in high concentrations in the root nodules of legumes that establish a symbiosis with nitrogen-fixing bacteria. In analogy to hemoglobin and myoglobin, we have shown that different forms of Lb react not only with $NO^{\bullet}$, but also with so-called reactive nitrogen species derived from it, among others peroxynitrite and nitrite. Because of the wider active-site pocket, the rate constants measured in this work for $NO^{\bullet}$ and for nitrite binding to metLb are 1 order of magnitude larger than the corresponding values for binding of these species to metmyoglobin and methemoglobin. Moreover, we showed that reactive nitrogen species are able to react with two forms of Lb that are produced in vivo but that cannot bind oxygen: ferrylLb is reduced by $NO^{\bullet}$ and nitrite, and nitrosylLb is oxidized by peroxynitrite. The second-order rate constants of these reactions are on the order of 10^2, 10^6, and 10^5 M^{-1} s^{-1}, respectively. In all cases, the final reaction product is metLb, a further Lb form that has been detected in vivo. Since a specific reductase is active in nodules, which reduces metLb, reactive nitrogen species could contribute to the recycling of these inactive forms to regenerate deoxyLb, the oxygen-binding form of Lb.

Keywords Leghemoglobin · Nitric oxide · Peroxynitrite · Nitrite · Hemoglobin · Kinetics

S. Herold (✉)
Laboratorium für Anorganische Chemie,
Eidgenössische Technische Hochschule,
ETH Hönggerberg, 8093 Zurich, Switzerland
E-mail: herold@inorg.chem.ethz.ch
Tel.: +41-44-6322858
Fax: +41-44-6321090

A. Puppo
UMR CNRS-UNSA-INRA IPMSV, 400, Route des Chappes,
BP167, 06903 Sophia-Antipolis Cedex, France

Abbreviations EPR: Electron paramagnetic resonance · Hb: Hemoglobin · Lb: Leghemoglobin · $LbFeO_2$ (oxyLb): Oxyleghemoglobin · $LbFe^{II}NO$ (nitrosylLb): Nitrosylleghemoglobin · $LbFe^{IV}=O$ (ferrylLb): Oxoiron(IV)leghemoglobin · Mb: Myoglobin · MetLb: Iron(III)leghemoglobin · NOS: Nitric oxide synthase

Introduction

Leghemoglobin (Lb) is a hemoprotein present in high concentrations in the root nodules of legumes that establish a symbiosis with nitrogen-fixing bacteria [1]. The structure of this monomeric protein is very similar to those of mammalian myoglobins (Mbs), and of the two subunits of human hemoglobin (Hb) [2, 3]. However, Lbs have a significantly higher affinity for oxygen compared with vertebrate Mbs and Hbs [4]. This feature is essential for their physiological role. Indeed, the function of Lbs is to facilitate O_2 transport to the bacteroids, via reversible binding of O_2 to their reduced heme center, in an environment that contains only approximately 10 nM O_2 [1]. The low oxygen tension is essential for preventing O_2-mediated inhibition of bacteroidal nitrogenase.

Several years after the discovery of the various physiological functions of nitrogen monoxide in animals [5], it is now widely accepted that $NO^{\bullet}$ is also generated in plants and that it plays a central role in plant defense against pathogens [6]. Interestingly, it is assumed that plant pathogenesis and symbiosis can induce similar responses in plants. Indeed, it appears that symbiotic bacteria are initially identified as pathogens and that only in a second stage they interfere successfully with plant defense responses [7, 8]. An enzyme similar to animal nitric oxide synthase (NOS) has been identified in roots and nodules of a leguminous plant (*Lupinus albus*) [9], and thus it has been suggested that $NO^{\bullet}$ may have a function in the regulation of the symbiotic process [8]. The observation that a nitrosylleghemoglobin complex

($LbFe^{II}NO$, nitrosylLb) has been detected in soybean [10], cowpea [11], and alfalfa [8] nodules, supports the hypothesis that Lb may be exposed to $NO^{\bullet}$. Moreover, since superoxide is produced during infection of symbiotic bacteria [7], different Lb forms may also react with the strong oxidizing and nitrating agent peroxynitrite, generated from the diffusion-controlled reaction between $NO^{\bullet}$ and $O_2^{\bullet-}$ [12, 13].

In a preceding paper we reported that soybean oxyleghemoglobin ($LbFeO_2$, oxyLb) reacts with nitrogen monoxide and peroxynitrite/CO_2 with second-order rate constants on the order of 10^8 and 10^5 M^{-1} s^{-1}, respectively [14]; thus, oxyLb is able to scavenge any $NO^{\bullet}$ (and peroxynitrite) formed during the nodulation process and thereby may prevent the triggering of the $NO^{\bullet}$-mediated defense reactions. In this work, we have investigated the reactivity of other Lb forms, which may also be produced in vivo, with different reactive nitrogen species. In particular, we have studied nitrite and $NO^{\bullet}$ binding to iron(III)leghemoglobin (metLb), a protein form that has been directly detected in intact nodules attached to roots by UV–vis spectroscopy [15]. Moreover, we have shown that $NO^{\bullet}$ and nitrite can reduce oxoiron(IV)leghemoglobin ($LbFe^{IV}=O$, ferrylLb) to metLb. Finally, we present kinetics studies of the oxidation of $LbFe^{II}NO$ by peroxynitrite, in the absence and in the presence of CO_2. Also this reaction leads to the formation of metLb, which can be reduced by a metLb reductase to the bioactive form of Lb (i.e., deoxyLb) [16]. The second-order rate constants for all these reactions are compared with those of the corresponding reactions with horse heart Mb and human Hb, and differences are rationalized in terms of the structural differences among the proteins.

Materials and methods

Reagents

Buffer solutions were prepared from K_2HPO_4/KH_2PO_4 (Fluka) with deionized Milli-Q water. Sodium dithionite, potassium superoxide, sodium nitrite, and hydrogen peroxide were obtained from Fluka. Nitrogen monoxide (Linde) was passed through a NaOH solution and a column of NaOH pellets before use in order to remove higher nitrogen oxides. Aqueous saturated nitrogen monoxide solutions (2 mM) were prepared as described previously [17]. The $NO^{\bullet}$-saturated stock solutions used for the synthesis of $LbFe^{II}NO$ by reductive nitrosylation of metLb (see later) were prepared in 0.1 M phosphate buffer pH 7.0–8.7. The concentration of these solutions is slightly lower than 2 mM.

Peroxynitrite, carbon dioxide, and proteins

Peroxynitrite was prepared either from KO_2 and gaseous nitrogen monoxide according to the method of Koppenol et al. [18] or by treating tetramethylammonium superoxide with nitrogen monoxide at –77 °C in liquid ammonia, followed by isolation as a crystalline solid via removal of the ammonia [19]. No difference was observed between the reactivity of peroxynitrite prepared according to the two procedures. The peroxynitrite solutions, which contained variable amounts of nitrite (0–50% relative to the peroxynitrite concentration) and no hydrogen peroxide, were stored in small aliquots at –80 °C. Nitrite contaminations did not interfere with our studies, since nitrite reacts with $LbFe^{II}NO$ at an extremely slow rate (on the order of 10^{-3} M^{-1} s^{-1}; S. Herold, unpublished results). The stock solutions were diluted either with 0.01 M NaOH or with water and the concentration of peroxynitrite was determined spectrophotometrically prior to each experiment by measuring the absorbance of the solutions at 302 nm ($\varepsilon_{302}=1{,}705$ M^{-1} cm^{-1}) [19].

For the experiments carried out in the absence of added CO_2, the buffers and the 0.01 M NaOH solutions were prepared fresh daily and thoroughly degassed. Experiments in the presence of CO_2 were carried out by adding the required amount of a freshly prepared 0.5 M sodium bicarbonate solution to the protein solutions as described in detail in Ref. [20]. The values for the constant of the hydration–dehydration equilibrium $CO_2 + H_2O \rightleftharpoons H^+ + HCO_3^-$ were taken from Ref. [21], by considering the ionic strength of the solutions. After addition of CO_2 or bicarbonate, the protein solutions were allowed to equilibrate at room temperature for at least 5 min.

Soybeans (*Glycine max*) were grown in a glasshouse and the Lb components purified from the root nodules as described previously [22]. All the experiments reported here were carried out with Lb c_2. The metLb concentration was determined by measuring the absorbance in 0.1 M phosphate buffer pH 7.0–7.3 at 404 nm ($\varepsilon_{404}=141$ mM^{-1} cm^{-1}). FerrylLb solutions were prepared as described in Ref. [23] and their concentration was determined by measuring the absorbance at 416 or 543 nm ($\varepsilon_{416}=97.2$ mM^{-1} cm^{-1} and $\varepsilon_{543}=10.4$ mM^{-1} cm^{-1}) [23]. NitrosylLb was prepared by reductive nitrosylation of metLb. In brief, a metLb solution (50 μM) kept over ice was thoroughly degassed by passing Ar over it for several hours or overnight. A large excess of $NO^{\bullet}$ (20–40 equiv) was added from a saturated stock solution in phosphate buffer pH 7.0–8.7. The reaction was carried out in a sealable cell for anaerobic applications and followed spectrophotometrically. When all $LbFe^{III}NO$ had been reduced to $LbFe^{II}NO$, the excess $NO^{\bullet}$ was removed by degassing the solution thoroughly with Ar.

UV-vis spectroscopy

Absorption spectra were collected in 1-cm cells with a UVIKON 820 spectrophotometer. Kinetics studies of the reductive nitrosylation of metLb were carried out with an Analytik Jena Specord 200. These studies were

performed in sealable cells for anaerobic applications (Hellma) in 0.05 M phosphate buffer pH 6.0–8.0 at room temperature (cell length 1 cm). The metLb solution (0.7 ml of a 2–5 μM solution in 0.1 M phosphate buffer) was placed in the sealable cell and thoroughly degassed at 0 °C by passing a flow of Ar over the surface of the solution for several hours (under constant stirring). The solution was then allowed to warm up to room temperature (under Ar). Finally, 0.7 ml of a 2 mM saturated aqueous $NO^{\bullet}$ solution was added with a SampleLock Hamilton syringe (final $NO^{\bullet}$ concentration 1 mM) and the measurement was started within 10 s. Spectra were collected every 60 s either in the Soret (400–450 nm) or in the visible (450–650 nm) region. The final pH was measured at the end of the reaction after removing excess $NO^{\bullet}$ by degassing the sample with Ar.

Stopped-flow kinetics analysis

Single-wavelength stopped-flow studies were carried out with an Applied Photophysics SX17MV or an SX18MV-R instrument. The measured reaction time courses were analyzed with Kaleidagraph, version 3.6.2. Rapid-scan spectrophotometric studies were performed with an On-Line Instrument Systems stopped-flow instrument equipped with an OLIS RSM 1000 rapid-scanning monochromator. The length of the cells in the three spectrophotometers was 1 cm. The mixing time of the instruments was 2–4 ms. If not specified, measurements were carried out at 20 °C. All the rate constants are expressed per heme.

Kinetics studies of the reaction of metLb with nitrite were carried out under pseudo-first-order conditions with nitrite in excess with the Applied Photophysics instruments. Reaction time courses were collected at different wavelengths between 400 and 440 nm. For the determination of the second-order rate constant the traces were mostly collected at 405 and/or 415 nm. For this purpose, the nitrite and metLb solutions were prepared under aerobic conditions in 0.1 M phosphate buffer pH 7.3.

The reaction between metLb and $NO^{\bullet}$ was first studied by rapid-scan stopped-flow spectroscopy in 0.1 M phosphate buffer pH 7.3. The second-order rate constant was then determined by single-wavelength measurements at 405 and/or 420 nm. The anaerobic metLb solution was prepared by thoroughly degassing it with Ar at 0 °C. The $NO^{\bullet}$ solutions were prepared by diluting the aqueous stock solution (2 mM) with degassed 0.1 M phosphate buffer directly in a SampleLock Hamilton syringe.

The reactions of ferrylLb with nitrogen monoxide and nitrite were first studied by rapid-scan stopped-flow spectroscopy in 0.1 M phosphate buffer pH 7.0. However, because of the large reaction rates kinetics studies of the $NO^{\bullet}$-mediated reduction of ferrylLb had to be carried out with the single-wavelength instrument (at 405 nm), which has a shorter mixing time and is more suited for measurements of very fast reactions. The second-order rate constants were determined under anaerobic conditions with ferrylLb in excess. In contrast, the second-order rate constant of the reaction between nitrite and ferrrylLb was determined under pseudo-first-order conditions with nitrite in excess, by following the absorbance changes at 405 nm.

Finally, the reaction of peroxynitrite with $LbFe^{II}NO$ was studied in 0.05 M phosphate buffer pH 7.3 under anaerobic conditions, both in the absence and in the presence of 1 mM CO_2. The protein solutions of the required concentrations were prepared by diluting the $LbFe^{II}NO$ stock solutions under aerobic conditions in degassed 0.1 M phosphate buffer. In general the pH of the buffer was slightly lower than the desired final pH, since upon mixing with the alkaline peroxynitrite solution the pH always rose between 0.2 and 0.4 units. The final pH was always measured at the end of the reactions for control. The reactions, carried out under pseudo-first-order conditions with peroxynitrite in excess, were first studied by rapid-scan spectroscopy. The second-order rate constants were determined by fitting the reaction time courses measured at 547 nm. Because of the large reaction rates, the kinetics of the reaction in the presence of CO_2 had to be measured with the single-wavelength instrument.

Statistics

The experiments reported in this article were carried out at least in triplicate on independent days. The results of the fits of the traces (averages of at least five to eight single traces) from at least three experiments were averaged to obtain each observed rate constant, given with the corresponding standard deviation.

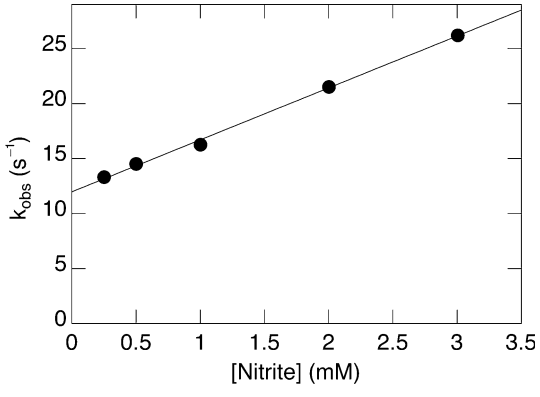

Fig. 1 Determination of the second-order rate constant for nitrite binding to iron(III)leghemoglobin (*metLb*). k_{obs} versus nitrite concentration for the reaction between metLb (3.6 μM) and nitrite, followed at 405 or 415 nm, in 0.05 M phosphate buffer pH 7.3 at 20 °C

Results

Kinetics studies of the reaction of metLb with nitrite

The reaction between nitrite and metLb was studied by stopped-flow spectroscopy at pH 7.3 and 20 °C by following the absorbance changes at 405 and/or 415 nm. The concentration of nitrite was always kept in a large excess to maintain pseudo-first-order conditions. All reaction time courses could be fitted well to a single-exponential expression (data not shown). As displayed in Fig. 1, a linear dependence was obtained between the observed rate constants and the nitrite concentration. The second-order rate constant determined from the linear fit is $(4.7 \pm 0.1)\times10^3$ M^{-1} s^{-1}, a value 1–2 orders of magnitude larger than those reported for nitrite binding to metMb and to the α- and the β-subunits of metHb (Table 1) [24, 25].

The rate constant for nitrite dissociation from $LbFe^{III}NO_2$, determined from the *y*-axis intercept of the plot shown in Fig. 1, is 12.0 ± 0.2 s^{-1}. Despite the error that may be associated with this indirect determination of the dissociation rate, the value obtained for $LbFe^{III}NO_2$ is significantly larger than those for the α- and the β-subunits of $HbFe^{III}NO_2$ (Table 1) [25]. In contrast, dissociation of nitrite from $MbFe^{III}NO_2$ is only slightly slower than from $LbFe^{III}NO_2$. Taken together, these kinetics data suggest that nitrite is a better ligand for metLb and metHb than for metMb.

To determine the UV-vis spectrum of $LbFe^{III}NO_2$ we mixed metLb with a very large excess of nitrite (approximately 1,000 equiv). Because NO_2^- has an absorbance maximum at 354 nm ($\varepsilon_{354}\approx23$ M^{-1} cm^{-1}), to obtain a spectrum of the Soret band of $LbFe^{III}NO_2$ we had to subtract the spectrum of nitrite measured under identical conditions. $LbFe^{III}NO_2$ displays absorbance maxima at 410 ($\varepsilon_{410} = 127$ mM^{-1} cm^{-1}) and 538 nm ($\varepsilon_{538} = 10.9$ mM^{-1} cm^{-1}), nearly identical to those of the corresponding human Hb complex $HbFe^{III}NO_2$ (Table 2) [26]. These spectroscopic features are typical for a low-spin iron(III) complex. In contrast, the nitrite complex of horse heart metMb displays absorbance maxima characteristic for a mixed low-spin/high-spin iron(III) complex (Table 2) [26].

Table 1 Comparison of rate constants for the reactions of leghemoglobin (*Lb*), human hemoglobin (*Hb*) and horse heart myoglobin (*Mb*) with various ligands at pH 7.0–7.5 and 20–25 °C

Protein	Reaction	Rate constants	Reference
Lb	$Fe(III) + NO_2^- \rightarrow Fe(III)NO_2$	$k_{on} = (4.7 \pm 0.1)\times10^3$ M^{-1} s^{-1} $k_{off} = 12.0 \pm 0.2$ s^{-1}	This study
Lb	$Fe(III) + NO^\bullet \rightarrow Fe(III)NO$	$k_{on} = (1.43 \pm 0.05)\times10^5$ M^{-1} s^{-1} $k_{off} = 3 \pm 1$ s^{-1}	This study
Lb	$Fe(III)NO + H_2O/HO^- + NO^\bullet \rightarrow Fe(II)NO + NO_2^- + 2H^+$	$k_{HO^-} = (3.3 \pm 0.2) \times 10^3$ $M^{-1}s^{-1}$ $k_{H_2O} = (3.0 \pm 0.9) \times 10^{-4}$ s^{-1}	This study
Lb	$Fe(IV)=O + NO_2^- \rightarrow Fe(III) + NO_3^-$	$k = (2.1 \pm 0.2)\times10^2$ M^{-1} s^{-1}	This study
Lb	$Fe(IV)=O + NO^\bullet \rightarrow Fe(III)ONO$ $Fe(III)ONO \rightarrow Fe(III) + NO_2^-$	$k = (1.8 \pm 0.1)\times10^6$ M^{-1} s^{-1} $k > 50$ s^{-1}	This study
Lb	$Fe(II)NO + HOONO/ONOO^- \rightarrow Fe(III)NO$ In the presence of 1 mM CO_2	$k = (8.8 \pm 0.2)\times10^3$ M^{-1} s^{-1} $k = (1.2 \pm 0.2)\times10^5$ M^{-1} s^{-1}	This study
Hb	$Fe(III) + NO_2^- \rightarrow Fe(III)NO_2$	$k_{on,\alpha} = (2.3 \pm 0.1)\times10$ M^{-1} s^{-1} $k_{on,\beta} = (1.4 \pm 0.1)\times10^2$ M^{-1} s^{-1} $k_{off,\alpha} = 0.12 \pm 0.01$ s^{-1} $k_{off,\beta} = 0.27 \pm 0.01$ s^{-1}	[25]
Hb	$Fe(III) + NO^\bullet \rightarrow Fe(III)NO$	$k_{on,\alpha} = 1.71\times10^3$ M^{-1} s^{-1} $k_{on,\beta} = 6.4\times10^3$ M^{-1} s^{-1} $k_{off,\alpha} = 1.5$ s^{-1} $k_{off,\beta} = 0.65$ s^{-1}	[27]
Hb	$Fe(III)NO + H_2O + NO^\bullet \rightarrow Fe(II)NO + NO_2^- + 2H^+$	$k_{HO^-} = 3.2 \times 10^3$ $M^{-1}s^{-1}$ $k_{H_2O} = 1.1 \times 10^{-3}$ s^{-1}	[29]
Hb	$Fe(IV)=O + NO_2^- \rightarrow Fe(III) + NO_3^-$	$k = (7.5 \pm 0.4)\times10^2$ M^{-1} s^{-1}	[25]
Hb	$Fe(IV)=O + NO^\bullet \rightarrow Fe(III)ONO$ $Fe(III)ONO \rightarrow Fe(III) + NO_2^-$	$k = (24 \pm 2)\times10^6$ M^{-1} s^{-1} $k_{fast} = (0.5 \pm 0.1)$ s^{-1} $k_{slow} = (0.12 \pm 0.04)$ s^{-1}	[25]
Hb	$Fe(II)NO + HOONO/ONOO^- \rightarrow Fe(III)NO$ In the presence of 1.2 mM CO_2	$k = (6.1 \pm 0.4)\times10^3$ M^{-1} s^{-1} $k = (5.3 \pm 0.2)\times10^4$ M^{-1} s^{-1}	[30]
Mb	$Fe(III) + NO_2^- \rightarrow Fe(III)NO_2$	$k_{on} = (3.2 \pm 0.1)\times10$ M^{-1} s^{-1} $k_{off} = 4.0 \pm 0.2$ s^{-1}	[24]
Mb	$Fe(III) + NO^\bullet \rightarrow Fe(III)NO$	$k_{on} = (2.7 \pm 0.1)\times10^4$ M^{-1} s^{-1} $k_{off} = 16.0 \pm 0.4$ s^{-1}	[28]
Mb	$Fe(III)NO + H_2O + NO^\bullet \rightarrow Fe(II)NO + NO_2^- + 2H^+$	$k_{HO^-} = (3.2 \pm 0.2) \times 10^2$ $M^{-1}s^{-1}$	[29]
Mb	$Fe(IV)=O + NO_2^- \rightarrow Fe(III) + NO_3^-$	$k = (16 \pm 1)$ M^{-1} s^{-1}	[24]
Mb	$Fe(IV)=O + NO^\bullet \rightarrow Fe(III)ONO$ $Fe(III)ONO \rightarrow Fe(III) + NO_2^-$	$k = (17.1 \pm 0.3)\times10^6$ M^{-1} s^{-1} $k = (5.98 \pm 0.06)$ s^{-1}	[24]

Table 2 Spectroscopic data for Lb, human Hb, and horse heart Mb complexes

	Soret	Visible		Reference
	$\lambda_{max}(\varepsilon)^a$	$\lambda_{max}(\varepsilon)^a$	$\lambda_{max}(\varepsilon)^a$	
$LbFe^{III}NO_2$	410 (127)	538 (10.9)	569 sh	This work
$LbFe^{III}NO$	420 (147)	533 (11.7)	567 (13.0)	This work
$LbFe^{II}NO$	418 (137)	546 (10.6)	570 (11.3)	This work
$HbFe^{III}NO_2$	411 (132)	538 (10.0)	567 sh	[26]
$HbFe^{III}NO$	415 (126)	533 (11.7)	566 (11.0)	[60]
$HbFe^{II}NO$	418 (130)	545 (12.6)	575 (13.0)	[61]
$MbFe^{III}NO_2$	412 (137)	502 (8.4)	573 (5.4) 628 (4.2)	[26]
$MbFe^{III}NO$	421 (150)	532 (12.7)	574 (12.5)	[60]
$MbFe^{II}NO$	418 (130)	546 (10.9)	579 (9.9)	[60]

[a] λ_{max} in nanometers; ε in per millimolar per centimeter

Kinetics studies of the reaction of metLb with nitrogen monoxide

The reaction between metLb and $NO^{\bullet}$ was studied by rapid-scan stopped-flow spectroscopy under anaerobic conditions at pH 7.3 and 20 °C. As shown in Fig. 2a, upon reaction with an excess of $NO^{\bullet}$ the absorbance maximum of the Soret band of metLb ($\lambda_{max} = 404$ nm, thin line) shifted to that of $LbFe^{III}NO$ ($\lambda_{max} = 420$ nm, bold line). Two isosbestic points were clearly visible during this process at 412 and 440 nm, respectively. As shown in Fig. 2b, in the visible range of the spectrum we also observed the transition of metLb ($\lambda_{max} = 532$ and 623 nm, thin line) to $LbFe^{III}NO$ ($\lambda_{max} = 533$ and 567 nm, bold line). The values of the extinction coefficients of $LbFe^{III}NO$, determined from the last spectra of the two experiments depicted in Fig. 2 are $\varepsilon_{420} = 147\ mM^{-1}\ cm^{-1}$, $\varepsilon_{533} = 11.7\ mM^{-1}\ cm^{-1}$, and $\varepsilon_{567} = 13.0\ mM^{-1}\ cm^{-1}$. Note that the maxima and the intensities of the absorbance bands of human $HbFe^{III}NO$ and horse heart $MbFe^{III}NO$ are comparable to those of $LbFe^{III}NO$ (Table 2).

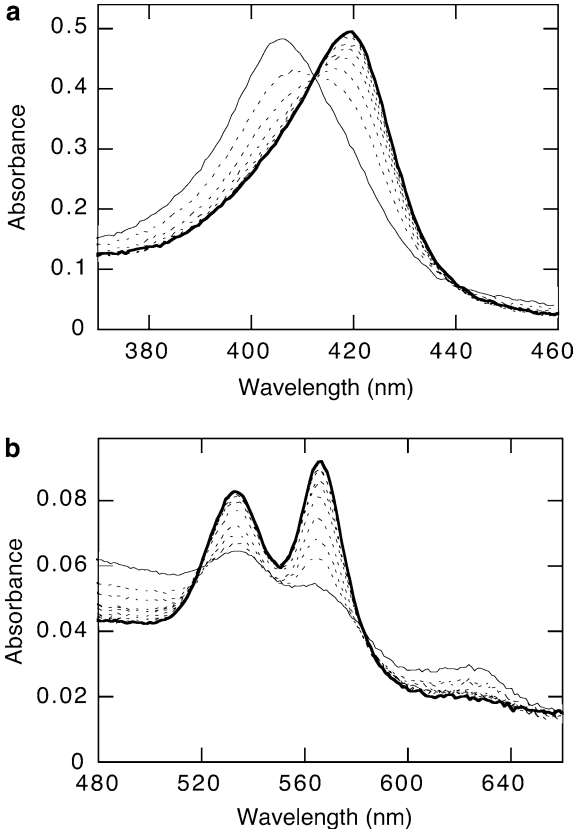

Fig. 2 Rapid-scan UV–vis spectra of the reaction of metLb with $NO^{\bullet}$ in 0.1 M phosphate buffer pH 7.3, 20 °C. Gradual conversion of metLb (*thin line*) to $LbFe^{III}NO$ (*bold line*). **a** Reaction of 3.4 μM metLb with 130 μM $NO^{\bullet}$. The spectra shown were collected with a time interval of 20 ms. **b** Reaction of 7.1 μM metLb with 100 μM $NO^{\bullet}$. The spectra shown were collected with a time interval of 40 ms

The second-order rate constant for $NO^{\bullet}$ binding to metLb was measured under pseudo-first-order conditions with $NO^{\bullet}$ in excess by following the absorbance changes at 405 and/or 420 nm, the maxima of metLb and $LbFe^{III}NO$, respectively. All reaction time courses could be fitted well to a single-exponential expression (data not shown). As depicted in Fig. 3, the observed rate constants increased linearly with increasing $NO^{\bullet}$ concentration. The second-order rate constant obtained from the linear fit is $(1.43 \pm 0.05) \times 10^5\ M^{-1}\ s^{-1}$, at pH 7.0 and 20 °C. Also in this case, the corresponding values of the rate constants for the reactions of $NO^{\bullet}$ with human metHb and horse heart metMb are 1–2 orders of

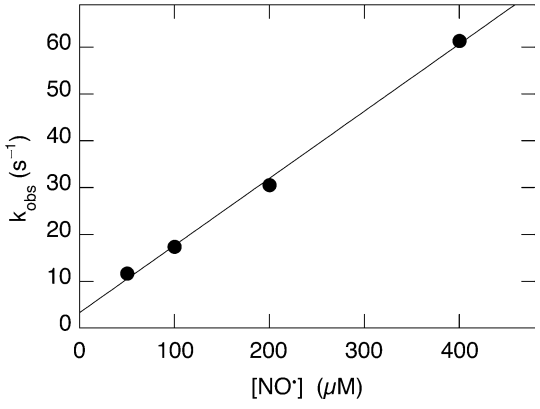

Fig. 3 Determination of the second-order rate constant for $NO^{\bullet}$ binding to metLb. k_{obs} versus $NO^{\bullet}$ concentration for the reaction between metLb (3.6 μM) and $NO^{\bullet}$, followed at 405 or 420 nm, in 0.05 M phosphate buffer pH 7.3 at 20 °C

magnitude lower (Table 1) [27, 28]. The rate constant of $NO^{\bullet}$ dissociation from $LbFe^{III}NO$ was extrapolated from the *y*-axis intercept of the fitted line of Fig. 3. Despite the large error associated with this value, ($3 \pm 1\ s^{-1}$), it is evident that the $NO^{\bullet}$ dissociation rate from $MbFe^{III}NO$ is significantly larger, whereas that from $HbFe^{III}NO$ is on the same order of magnitude.

Reductive nitrosylation of metLb

Figure 4 shows the absorbance changes observed when metLb was mixed with a large excess of $NO^{\bullet}$ at pH 7.0 and 20 °C. The absorbance maxima characteristic for $LbFe^{III}NO$ (420, 533, and 567 nm, dotted bold lines), the species formed immediately after addition of 50–250 equiv $NO^{\bullet}$ to metLb (thin line), gradually shifted to 418, 546, and 570 nm (bold line). These maxima are identical to those obtained upon addition of $NO^{\bullet}$ to deoxyLb, and are very similar to those of $HbFe^{II}NO$ and $MbFe^{II}NO$ (Table 2). The extinction coefficients of the absorbance maxima of the $LbFe^{II}NO$ spectrum, determined from the last spectra in Fig. 4 ($\varepsilon_{418} = 137\ mM^{-1}\ cm^{-1}$, $\varepsilon_{546} = 10.6\ mM^{-1}\ cm^{-1}$, and $\varepsilon_{570} = 11.3\ mM^{-1}\ cm^{-1}$), are comparable to those of the corresponding Hb and Mb complexes (Table 2). Thus this experiment indicates that $LbFe^{III}NO$ undergoes reductive nitrosylation to produce $LbFe^{II}NO$ (Eqs. 1, 2, 3).

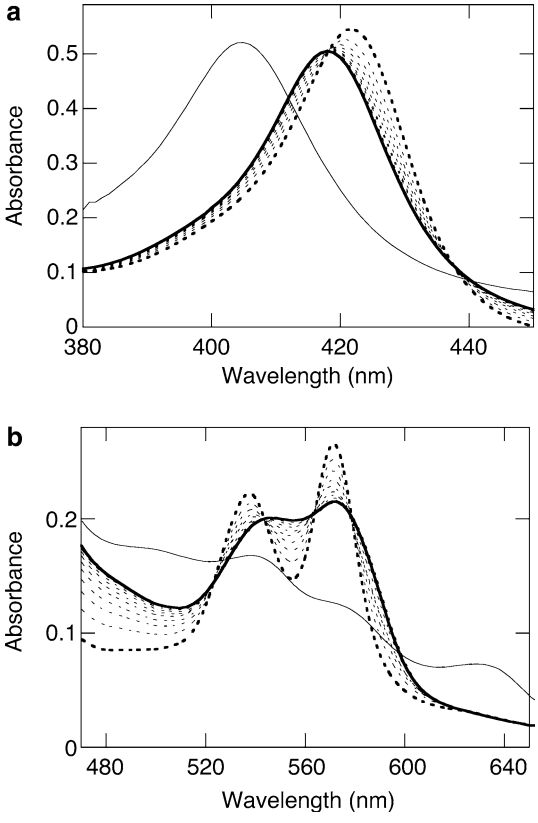

Fig. 4 Reductive nitrosylation of metLb. Rapid-scan UV–vis spectra of the reaction of metLb with excess $NO^{\bullet}$ in 0.1 M phosphate buffer pH 7.0, 20 °C. The immediate conversion of metLb (*thin line*) to $LbFe^{III}NO$ (*bold dotted line*) and its slow transformation to $LbFe^{II}NO$ (*bold line*) are shown. The spectra were collected every 10 min. **a** Reaction of 3.7 μM metLb with 1 mM $NO^{\bullet}$. **b** Reaction of 20 μM metLb with 1 mM $NO^{\bullet}$

$$LbFe^{III} + NO^{\bullet} \rightleftarrows LbFe^{III}NO \leftrightarrow LbFe^{II}(NO^{+}) \quad (1)$$

$$LbFe^{III}NO + H_2O/HO^{-} \rightarrow LbFe^{II} + NO_2^{-} + 2H^{+} \quad (2)$$

$$LbFe^{II} + NO^{\bullet} \rightarrow LbFe^{II}NO \quad (3)$$

The rate of reductive nitrosylation was determined by fitting the traces extracted at 421 and/or 570 nm. At all wavelengths measured, the reaction time courses could be fitted well to a single-exponential expression (data not shown). At pH 7.0 and room temperature we obtained an observed rate of $(4.8 \pm 0.2) \times 10^{-4}\ s^{-1}$. Analogous experiments were carried out at different pH values in the range 6.0–8.0. The kinetics traces could all be fitted well to a single-exponential expression and the observed rate constants increased with increasing pH. Moreover, we found that the observed rate of reductive nitrosylation did not depend on the protein concentration in the range 3–20 μM metLb.

Since reductive nitrosylation also occurred under acidic conditions, our results suggest that $LbFe^{III}NO$ reacts not only with HO^{-} but also with H_2O (Eq. 2). In all cases, binding of $NO^{\bullet}$ to $LbFe^{II}$ is very fast, and therefore $LbFe^{ii}$ is never observed and Eq. 2 represents the rate-determining step. Thus, as observed experimentally, it is expected that the rate of $LbFe^{II}NO$ formation follows first-order kinetics. The expression for the observed rate constant, which depends on the $NO^{\bullet}$ concentration, can be derived from the reaction scheme (Eqs. 1, 2, 3): $k_{obs} = k'_{HO^-} \times K_{eq} \times [NO^{\bullet}] / (1 + K_{eq} \times [NO^{\bullet}])$, where $k'_{HO^-} = k_{HO^-} \rightarrow [HO^-] + k_{H_2O}$ and K_{eq} is the equilibrium constant for $NO^{\bullet}$ binding to metLb ($4.8 \times 10^4\ M^{-1}$, see earlier). The two terms k_{HO^-} and k_{H_2O} are the second-order rate constant for the reaction between $LbFe^{III}NO$ and HO^{-} and the observed rate

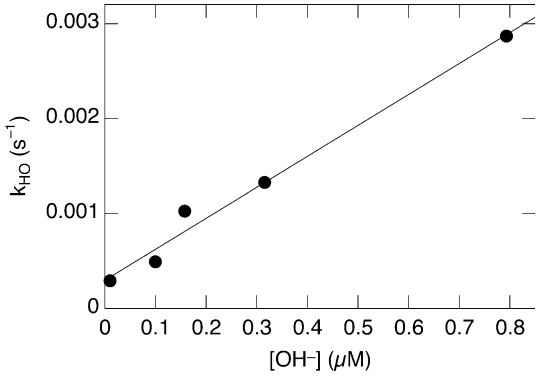

Fig. 5 Determination of the second-order rate constant for the reaction between OH^{-} and $LbFe^{III}NO$ in the presence of excess $NO^{\bullet}$. k'_{HO^-} versus OH^{-} concentration for the conversion of $LbFe^{III}NO$ to $LbFe^{II}NO$, followed at 421 or 570 nm, in 0.05 M phosphate buffer pH 6.0–8.0, at room temperature

constant for the reaction of $LbFe^{III}NO$ with H_2O, respectively. The $NO^{\bullet}$ concentration used in the experiments was always 1 mM; thus, one can calculate that $k'_{HO^-} = k_{obs}/0.98$. As shown in Fig. 5, the plot of k'_{HO^-} versus HO^- concentration gave a straight line with a positive intercept. From the slope and the *y*-axis intercept of the linear fit we obtained the values of $k_{HO^-} = (3.3 \pm 0.2) \times 10^3\ M^{-1}s^{-1}$ and $k_{H_2O} = (3.0 \pm 0.9) \times 10^{-4}\ s^{-1}$. The value of k_{HO^-} is identical to that reported for human Hb [29]. In contrast, the value of k_{H_2O} is 3–4 times lower than that found for human Hb ($k_{H_2O} = 1.1 \times 10^{-3}\ s^{-1}$) [29]. Interestingly, $MbFe^{III}NO$ does not react with H_2O but only with HO^-, and this process takes place at a significantly higher rate (Table 1) [29].

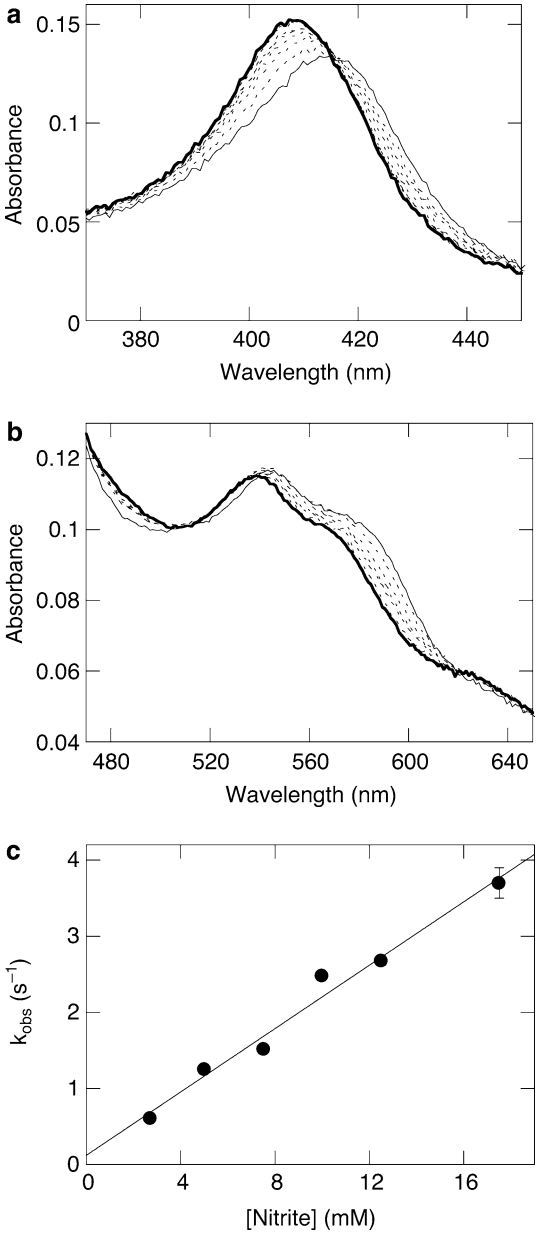

Fig. 6 Rapid-scan UV-vis spectra of the reaction of oxoiron(IV)leghemoglobin (*ferrylLb*) with excess NO_2^- in 0.1 M phosphate buffer pH 7.0, 20 °C. The conversion of ferrylLb (*thin line*) to $LbFe^{III}NO_2^-$ (*bold line*) is shown. **a** Reaction of 1.3 μM ferrylLb with 2.7 mM nitrite. The spectra were collected every 500 ms. For clarity, the absorbance arising from nitrite (λ_{max} = 354 nm) was substracted from each trace. **b** Reaction of 11 μM ferrylLb with 5.5 mM nitrite. The first five spectra were collected every 400 ms, whereas the last two spectra were collected with a time interval of 1.6 s. **c** k_{obs} versus NO_2^- concentration for the reduction of ferrylLb, followed at 405 nm in 0.1 M phosphate buffer pH 7.0 at 20 °C

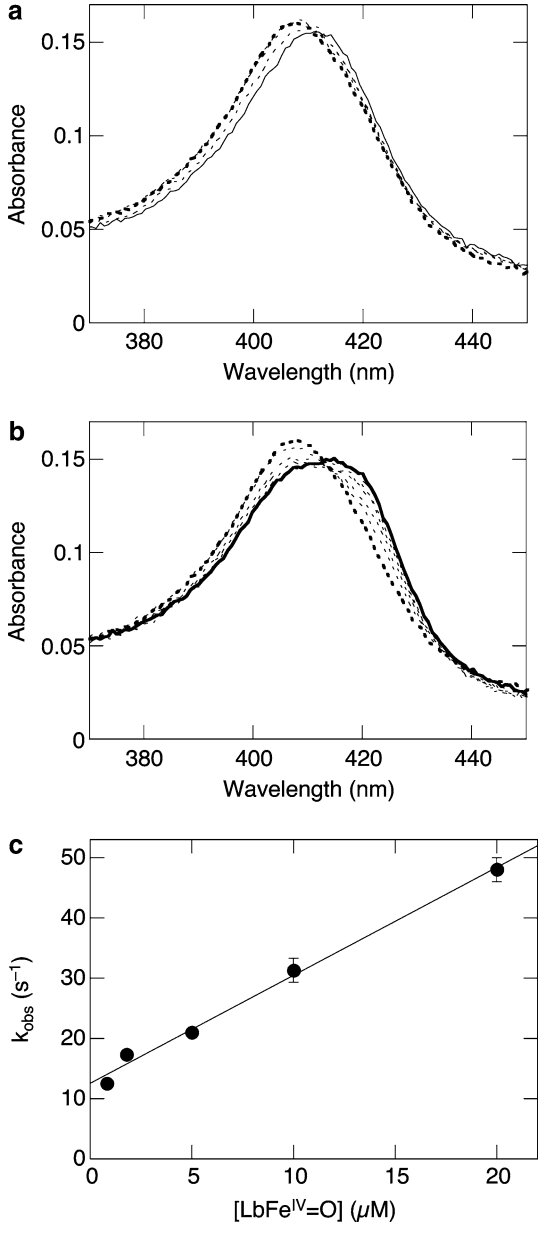

Fig. 7 Rapid-scan UV–vis spectra of the reaction of ferrylLb (1.2 μM) with excess $NO^{\bullet}$ (10 μM) in 0.1 M phosphate buffer pH 7.0, 20 °C. **a** Conversion of ferrylLb (*thin line*) to metLb (*bold dotted line*) and **b** subsequent partial binding of $NO^{\bullet}$ to yield a mixture of metLb and $LbFe^{III}NO$ (*bold line*). In **a** the spectra were collected every 20 ms and in **b** every 125 ms. **c** k_{obs} versus ferrylLb concentration for the reduction of ferrylLb, followed at 405 nm in 0.1 M phosphate buffer pH 7.0 at 20 °C

Kinetics studies of the reaction of ferrylLb with nitrite

Rapid-scan spectroscopic studies of the reaction between ferrylLb and an excess of nitrite were performed under aerobic conditions at pH 7.0 and 20 °C. As shown in Fig. 6a, addition of 2.7 mM nitrite to 1.3 μM ferrylLb led to the shift of the Soret band from 416 nm (λ_{max} of ferrylLb, thin line) to approximately 410 nm (bold line). This absorbance maximum corresponds to that of $LbFe^{III}NO_2$ (see earlier). Indeed, because of the large excess of nitrite used and because of the large value of the rate constant of nitrite binding to metLb (Table 1), the final reaction product is not metLb but $LbFe^{III}NO_2$. Indeed, under the conditions of the experiment depicted in Fig. 6a, the observed rate constant for nitrite binding to metLb is approximately 25 s^{-1} (Fig. 1), whereas the nitrite-mediated reduction of ferrylLb proceeds at a rate of approximately 0.6 s^{-1} (Fig. 6b). Thus, under these conditions it is not possible to detect metLb and the conversion of ferrylLb to $LbFe^{III}NO_2$ proceeds with a clean isosbestic point (at 415 nm, Fig. 6a). The reaction between nitrite and ferrylLb was also studied by following the absorbance changes in the visible range. As shown in Fig. 6b, the conversion of ferrylLb ($\lambda_{max} = 543$ nm, thin line) to $LbFe^{III}NO_2$ ($\lambda_{max} = 538$ nm, bold line) was also observed.

The second-order rate constant for the nitrite-mediated reduction of ferrylLb was determined by following the absorbance increase at 405 nm. All reaction time courses could be fitted well to a single-exponential expression (data not shown). The linear fit of the plot of k_{obs} versus nitrite concentration depicted in Fig. 6c gave a value of the second-order rate constant of $(2.1 \pm 0.2) \times 10^2$ M^{-1} s^{-1}. This value is slightly lower than that for the corresponding reaction with ferrylHb [25] but 1 order of magnitude larger than that with ferrylMb [24] (Table 1).

Kinetics studies of the reaction of ferrylLb with nitrogen monoxide

Rapid-scan spectroscopic studies of the reaction between ferrylLb (approximately 1 μM) and an excess of $NO^{\bullet}$ (approximately 10 μM) indicated that the first reaction product is metLb, which then partly binds excess $NO^{\bullet}$ to generate a mixture of metLb and $LbFe^{III}NO$. The reaction is very fast and thus the first

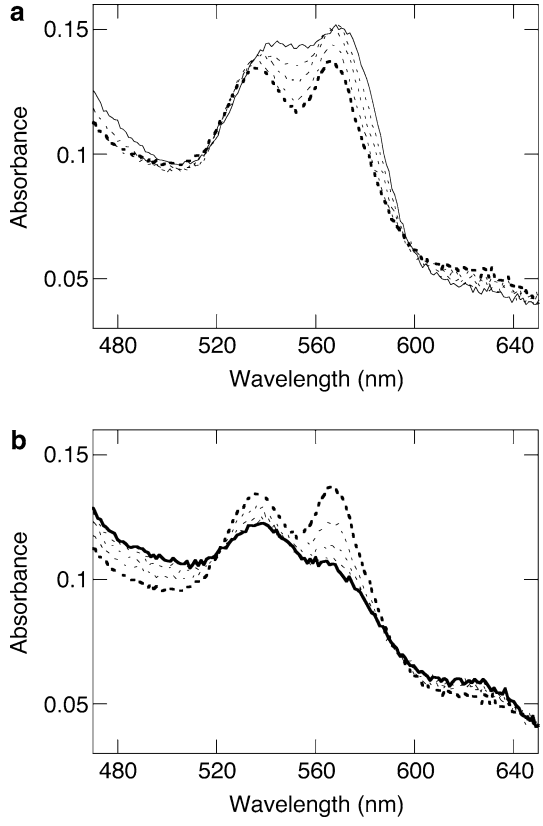

Fig. 8 Rapid-scan UV–vis spectra of the reaction of $LbFe^{II}NO$ (9 μM) with excess peroxynitrite (144 μM) in 0.1 M phosphate buffer pH 7.3, 20 °C. **a** The oxidation of $LbFe^{II}NO$ (*thin line*) to $LbFe^{III}NO$ (*bold dotted line*) and **b** its slow transformation to metLb (*bold line*). In **a** the spectra were collected every 200 ms and in **b** every 400 ms

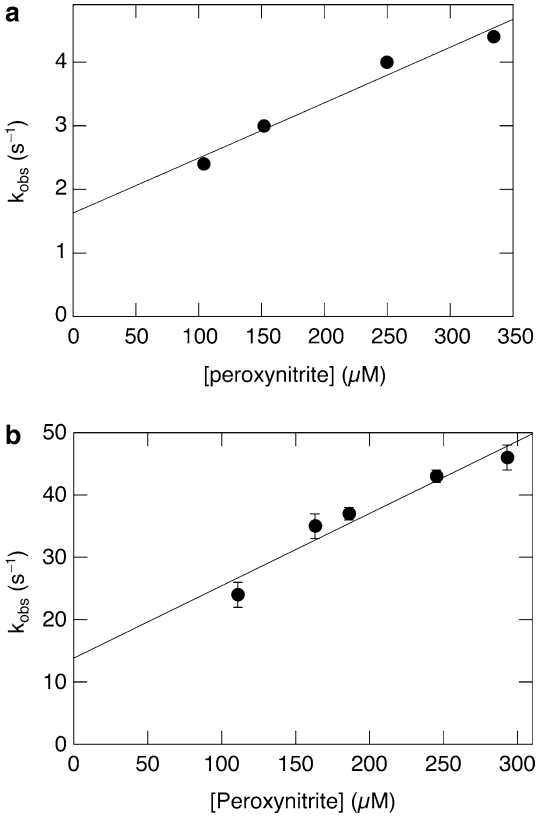

Fig. 9 k_{obs} versus peroxynitrite concentration for the oxidation of $LbFe^{II}NO$ (approximately 9 μM) to $LbFe^{III}NO$ in 0.1 M phosphate buffer pH 7.3, 20 °C. **a** In the absence and **b** in the presence of 1.2. mM CO_2

spectrum measured ($\lambda_{max} = 411$ nm, thin line in Fig. 7a) represents that of a mixture of ferrylLb ($\lambda_{max} = 416$ nm) and metLb ($\lambda_{max} = 404$ nm). Under the conditions of the experiment depicted in Fig. 8a and b, binding of $NO^{\bullet}$ to metLb produced from the first reactions step proceeds at a rate of approximately 5 s^{-1}, a value 6 times lower than that for the $NO^{\bullet}$-mediated reduction of ferrylLb (31 s^{-1}). However, the spectrum of pure metLb was never observed. Indeed, the spectrum with an absorbance maximum at the lowest wavelength, shown as a dotted bold line in Fig. 8a and b, has a λ_{max} of 407 nm. The last spectrum, shown as a bold line in Fig. 7b, is that of a mixture of metLb and $LbFe^{III}NO$. The second-order rate constant of the $NO^{\bullet}$-mediated reduction of ferrylLb was determined by single-wavelength stopped-flow spectroscopy at pH 7.0 and 20 °C. In order to avoid the difficulties associated with the accurate measurement of the $NO^{\bullet}$ solutions, the protein was present in tenfold excess to maintain pseudo-first-order conditions. With these settings the subsequent binding of $NO^{\bullet}$ to metLb could also be avoided. The reaction time courses, measured by following the absorbance increase at 405 nm, could all be fitted well to a single-exponential expression.

The second-order rate constants were determined by the fit of the linear plot of k_{obs} versus ferrylLb concentration (Fig. 7c). The value obtained, $(1.8 \pm 0.1) \times 10^6$ M^{-1} s^{-1}, is 1 order of magnitude smaller than those for the corresponding reactions of $NO^{\bullet}$ with ferrylHb and ferrylMb (Table 1) [24, 25].

In the pH range 6.0–9.5, the reactions of $NO^{\bullet}$ with ferrylHb and ferrylMb have been shown to proceed via the corresponding O-bound nitrite iron(III) complexes ($Fe^{III}ONO$), which have been characterized by UV–vis spectroscopy under alkaline conditions [24, 25]. Interestingly, under neutral conditions (pH 7.0) rapid-scan spectroscopic studies of the reaction of $NO^{\bullet}$ with ferrylLb did not show the presence of a detectable intermediate.

Kinetics studies of the reaction of $LbFe^{II}NO$ with peroxynitrite, in the absence and in the presence of 1 mM CO_2

The reaction between $LbFe^{II}NO$ and peroxynitrite was studied by rapid-scan stopped-flow spectroscopy under anaerobic conditions at pH 7.3 and 20 °C. As shown in Fig. 8a, upon addition of an excess of peroxynitrite the characteristic spectrum of $LbFe^{II}NO$ ($\lambda_{max} = 546$ and 570 nm, thin line) was converted into that of $LbFe^{III}NO$ ($\lambda_{max} = 533$ and 567 nm, bold dotted line). Over a longer time scale (Fig. 8b), the spectrum of $LbFe^{III}NO$ (bold dotted line) changed into that of metLb ($\lambda_{max} = 533$ nm, bold line). The reaction between $LbFe^{II}NO$ and peroxynitrite was also studied by following the absorbance changes of the Soret band. Also in this case, we observed a two-step reaction: the oxidation of $LbFe^{II}NO$ to $LbFe^{III}NO$, followed by $NO^{\bullet}$ dissociation to produce metLb (data not shown). An analogous reaction pathway has recently been observed for the corresponding reaction between $HbFe^{II}NO$ and peroxynitrite [30].

The kinetics of the two reaction steps were determined separately by fitting the reaction time courses measured at 547 and 566 nm for the first and the second processes, respectively. The reaction time courses (data not shown) could be fitted well to a single-exponential expression. However, the trace measured at 566 nm for the second process had to be fitted by starting from the point when the first reaction step was over (mostly around 1 s). The observed rate constants for the oxidation of $LbFe^{II}NO$ to $LbFe^{III}NO$ were found to depend linearly on the peroxynitrite concentration and the linear fit of the plot shown in Fig. 9a gave a value of the second-order rate constant of $(8.8 \pm 0.2) \times 10^3$ M^{-1} s^{-1}. This value is very similar to that recently determined for the corresponding peroxynitrite-mediated oxidation of $HbFe^{II}NO$ (Table 1) [30]. As expected, the rate of $NO^{\bullet}$ dissociation from $LbFe^{III}NO$ was independent of the peroxynitrite concentration. The value obtained, (2.0 ± 0.2) s^{-1}, is essentially identical to that extrapolated from the y-axis intercept of the linear fit of the plot of the observed rate constant for $NO^{\bullet}$ binding to metLb versus $NO^{\bullet}$ concentration (3 ± 1 s^{-1}; Fig. 5).

Interestingly, when the protein and the peroxynitrite concentrations were low (2 and 50 μM, respectively) a lag phase was observed at the beginning of the reaction time courses (data not shown). Moreover, kinetics traces of the reactions with high protein and peroxynitrite concentrations (10 and 250 μM, respectively) were not perfectly exponential, but had the tendency to be slightly linear (data not shown). Taken together, these observations suggest the presence of an autocatalytic process. Detailed studies with $MbFe^{II}NO$ and $HbFe^{II}NO$ (F. Boccini and S. Herold, unpublished results) showed that autocatalysis derives from the interaction of peroxynitrite with $NO^{\bullet}$ (dissociated from $Fe^{III}NO$), which leads to the formation of a species that can oxidize $MbFe^{II}NO$ and $HbFe^{II}NO$ at a faster rate than peroxynitrite. This complex mechanism may also explain the positive intercept of the plot of k_{obs} versus peroxynitrite concentration (Fig. 9a).

The reactivity of peroxynitrite in biological systems is known to be strongly influenced by CO_2 [13], which is present in millimolar concentration in the active root nodules [31]. Thus, the reaction between $LbFe^{II}NO$ and peroxynitrite was also studied in the presence of approximately 1 mM CO_2. Rapid-scan spectroscopic studies (data not shown) showed qualitatively the same absorbance changes as those observed for the reaction in the absence of CO_2 (Fig. 9a, b). The two wavelengths chosen to follow the reaction steps were 581 and 572 nm, respectively. From the linear fit of the plot of the observed rate constants versus peroxynitrite concentration (Fig. 9b), we obtained a second-order rate constant of $(1.2 \pm 0.2) \times 10^5$ M^{-1} s^{-1}. This value is slightly larger than that obtained for the analogous reactions of peroxynitrite with $HbFe^{II}NO$ (in the

presence of 1.2 mM CO_2; Table 1) [30]. As expected, the value of the observed rate constant for the second reaction step, $NO^{\bullet}$ dissociation from $LbFe^{II}NO$, was independent of the peroxynitrite concentration and was not influenced by addition of CO_2. Indeed, we obtained a value of $2.5 \pm 0.2\ s^{-1}$, essentially identical to that obtained in the absence of CO_2.

Discussion

The amino acid sequence of soybean Lb shows a high degree of homology with those of vertebrate Mbs and Hbs [1, 32]. Also its tertiary folding pattern is very similar to that of Mb and of the α- and the β-subunits of human Hb [2, 3]. Moreover, soybean Lb contains two histidine residues in positions analogous to those of the "proximal" and "distal" histidine of mammalian Hb and Mb. In these proteins, these two histidine residues are coordinated to the iron center and strongly hydrogen bonded to the coordinated oxygen (in oxyHb) or to the bound H_2O (in metHb), respectively. In contrast, kinetics studies with distal histidine Lb mutants (His61 in soybean Lb) [3] as well as spin-echo electron paramagnetic resonance (EPR) studies [33] showed that in oxyLb the hydrogen bond between the distal histidine and the coordinated O_2 is very weak at neutral pH and becomes strong only at low pH.

A further difference between the structures of Hb/Mb and Lb is the presence of a wider and more flexible heme pocket in Lb [2, 3]. This feature is reflected in the large values of the association rate constants for binding of bulky ligands such as long-chain alkylisocyanides to metLb: in some cases these ligands do not even bind to metMb [34, 35]. It has been shown that Lb binds these ligands more strongly that does Mb because the dissociation rates are lower for Lb complexes. This property has been proposed to arise principally from direct iron-to-ligand interactions, rather than possible ligand-to-protein secondary interactions [34].

A similar trend was observed in this work for the rate constants of nitrite and $NO^{\bullet}$ binding to metLb. For both ligands, the association rate constants are 1–2 orders of magnitude larger for the reactions with Lb compared with those with metHb and metMb (Table 1). The nitrite and $NO^{\bullet}$ dissociation rates from the corresponding metLb complexes are 2 orders of magnitude larger than those from metHb complexes, and approximately equivalent to those of metMb. Note that in this work the $NO^{\bullet}$ dissociation rate constants were extrapolated from the y-axis intercept in Fig. 4, and were not measured directly by using a ruthenium complex as a $NO^{\bullet}$ scavenger, as in the case of metMb [36].

Recent detailed kinetics studies of $NO^{\bullet}$ and nitrite binding to metMb have demonstrated that this reaction proceeds via a limiting dissociative ligand substitution mechanism [28, 36, 37]. In particular, the large positive values of the volume and the entropy of activation are consistent with a mechanism in which dissociation of the water molecule that occupies the sixth coordination site of metMb must precede formation of the Fe^{III}–NO or the Fe^{III}–NO_2^- bond [28, 36]. Studies of $NO^{\bullet}$ binding to distal histidine mutants of metMb have pointed out the important role of the hydrogen bond between the distal histidine and the coordinated water molecule [37]. Indeed, this strong interaction slows down the rate of $NO^{\bullet}$ binding to metMb by 3 orders of magnitude [37]. Taken together, our data confirm the enhanced reactivity of metLb due to a wider heme pocket, a more loosely bound water molecule in the sixth coordination site of metLb, and a weaker hydrogen bond between this water molecule and the distal histidine.

The UV–vis spectrum of the nitrite complex of Lb, $LbFe^{III}NO_2$, displays absorbance maxima typical for a low-spin heme-iron(III) complex. Nearly identical values of the absorbance maxima as well as of the extinction coefficients are observed for the corresponding human Hb complex $HbFe^{III}NO_2$ [26]. Interestingly, the spectrum of horse heart $MbFe^{III}NO_2$ shows features typical for a mixture of a high-spin (502 and 628 nm) and a low-spin (573 nm) heme-iron(III) complex [26].

In analogy to the corresponding metMb and metHb $NO^{\bullet}$ complexes, $LbFe^{III}NO$ undergoes reductive nitrosylation and, in the presence of excess $NO^{\bullet}$, this leads to the formation of $LbFe^{II}NO$. Interestingly, our work showed that with Lb this reaction also takes place under acidic conditions and thus not only OH^- but also H_2O can produce nitrite from $LbFe^{III}NO$. This result is comparable to that observed for $HbFe^{III}NO$ (Eq. 2). In contrast, $MbFe^{III}NO$ undergoes reductive nitrosylation only under basic conditions. It has been proposed that the difference in reactivity between the Mb and the Hb complexes may be due to the lower reduction potential of Mb [29]. Indeed, the mechanism of reductive nitrosylation has been rationalized in terms of a charge transfer from $NO^{\bullet}$ to Fe(III) to give $Fe^{II}(NO^+)$ (Eq. 1). The reduction potential of LbFe(III) is 0.22 V [38], a value rather close to that of Hb (0.17 V) and higher than that of Mb (0.06 V). Thus, a stabilization of $LbFe^{II}(NO^+)$ may explain why reductive nitrosylation also takes place under acidic conditions.

The ferryl form of Lb has been shown to be produced by reaction of H_2O_2 with deoxyLb [23], oxyLb [1], or metLb [39]; however, only the reaction between deoxyLb and H_2O_2 leads to the formation of the pure form of ferrylLb. All other reactions are accompanied by production of radical species [40, 41] and/or side products [42]. Sources of H_2O_2 in root nodules are, among others, the disproportionation of $O_2^{\bullet-}$ produced from autoxidation of oxyLb [43] or as a result of the strong reducing conditions required for N_2 fixation [44].

In contrast to ferrylHb [45], ferrylLb does not undergo synproportionation with oxyLb [46]. However, it has been suggested that ascorbate and glutathione, present in high concentrations in the nodule cytosol (approximately 2 mM and 100 μM, respectively [47]),

may reduce ferrylLb in vivo. Indeed, this form of Lb could not be detected in nodule extracts [46]. The in vitro reduction of ferrylLb by ascorbate and by glutathione has been shown to proceed at a rather slow rate (with a half-life on the order of several minutes) [39, 48].

Compared with ferrylMb, ferrylLb is significantly stabler and its UV–vis spectrum shows insignificant absorbance changes for over 12 h at 25 °C. Among others, it has been shown that, in contrast to ferrylMb and ferrylHb, ferrylLb does not react with H_2S and H_2O_2 [23]. Interestingly, in a preceding paper we showed that peroxynitrite is able to reduce ferrylLb to metLb. The second-order rate constants for this process are $(2.1 \pm 0.2)\times10^4$ and $(3.6 \pm 0.5)\times10^5$ M^{-1} s^{-1} for the reaction in the absence and in the presence of 1.2 mM CO_2, respectively [14]. In analogy to the reaction of peroxynitrite with ferrylMb [20, 49] and with ferrylHb [50], we have proposed that $NO_2^{\bullet}$, produced from the decay of peroxynitrite in particular in the presence of CO_2, is the reactive species in this process [14]. The reaction thus proceeds via the formation of a nitrato-iron(III) complex from which metLb and free nitrate are produced (Eq. 4):

$$\begin{aligned} \mathrm{LbFe^{IV}{=}O} + \mathrm{NO_2^{\bullet}} &\rightarrow \mathrm{LbFe^{III}ONO_2} \\ &\rightarrow \mathrm{LbFe^{III}} + \mathrm{NO_3^-}. \end{aligned} \tag{4}$$

In this work, we have shown that another reactive nitrogen species that can reduce ferrylLb to metLb very efficiently is $NO^{\bullet}$. Indeed, the value of the second-order rate constant for this reaction is on the order of 10^6 M^{-1} s^{-1} (Table 1). The corresponding values of the second-order rate constants of the reaction of $NO^{\bullet}$ with the more reactive ferrylMb [24] and ferrylHb [25] are 1 order of magnitude larger (Table 1). Interestingly, the *O*-nitrito-iron(III) intermediate (Eq. 5), which was detected spectroscopically for the reactions with ferrylMb [24] and ferrylHb [25], decayed too rapidly to be detected in the corresponding reaction with ferrylLb. Thus, dissociation of nitrite from $LbFe^{III}ONO$ must proceed at a rate larger than approximately 50 s^{-1}, the largest observed rate constant measured in our kinetics studies of the $NO^{\bullet}$-mediated reduction of ferrylLb (Fig. 7c). Under identical conditions, $MbFe^{III}ONO$ has been shown to decay to metMb and nitrite at a rate of 6.0 ± 0.4 s^{-1} [24]. The $HbFe^{III}ONO$ complex is stabler and the two subunits decay at rates of 0.5 ± 0.1 and 0.12 ± 0.04 s^{-1} [25]. These differences are probably again a consequence of the wider active-site pocket of Lb and are in line with the lack of detection of the metLb-peroxynitrite complex, the intermediate of the $NO^{\bullet}$-mediated oxidation of oxyLb [14]. Also in this case, the complex could be detected spectroscopically in the course of the corresponding reaction of $NO^{\bullet}$ with oxyMb and oxyHb [26, 51].

$$\mathrm{LbFe^{IV}{=}O} + \mathrm{NO^{\bullet}} \rightarrow \mathrm{LbFe^{III}ONO} \rightarrow \mathrm{LbFe^{III}} + \mathrm{NO_2^-} \tag{5}$$

We have previously shown that also nitrite can reduce ferrylMb and ferrylHb to the corresponding iron(III) species. Here we show that despite the higher stability of ferrylLb, the second-order rate constant of its reaction with nitrite is of the same order of magnitude as that of ferrylHb and 10 times larger than that of ferrylMb. However, because of the low nitrite content in nodules (in the micromolar range at most [52]), this reaction is not likely to be relevant *in planta*.

A further Lb form found in plants is $LbFe^{II}NO$, which has been proposed to be produced from the reaction of nitrite with deoxyLb [53], a process which probably proceeds as the corresponding reaction between deoxyHb and nitrite (Eqs. 6, 7) [54]. Indeed, nitrosylLb has been detected in extracts from root nodules of plants cultured with nitrate [55]. It has been proposed that the enzyme responsible for reduction of nitrate to nitrite is nitrate reductase, localized in the cytosol [55]. Interestingly, the reaction between deoxyHb and nitrite has recently attracted great interest, since it has been proposed to represent a pathway for $NO^{\bullet}$ production in blood under hypoxic conditions [56]. The same may hold for the reaction between nitrite and deoxyLb: together with $NO^{\bullet}$ production from NOS [9] and from the reduction of nitrite by nitrate reductase [57–59], this reaction may represent an unrecognized pathway for $NO^{\bullet}$ production in the nodules.

$$\mathrm{LbFe^{II}} + \mathrm{HONO} \rightarrow \mathrm{LbFe^{III}} + \mathrm{NO^{\bullet}} + \mathrm{OH^-} \tag{6}$$

$$\mathrm{LbFe^{II}} + \mathrm{NO^{\bullet}} \rightarrow \mathrm{LbFe^{III}NO}. \tag{7}$$

Nitrate has been reported to inhibit nodule growth and nitrogenase activity when it is supplied to soybean plants [55]. This inhibition process has been proposed to be a consequence of the generation of $LbFe^{II}NO$. Indeed, $LbFe^{II}NO$ is a stable Lb complex that does not undergo autoxidation and is not converted to oxyLb in the presence of dioxygen [11, 53]. Thus, formation of $LbFe^{II}NO$ inhibits the physiological function of Lb, that is reversible oxygen binding, and consequently leads to inhibition of nitrogenase and interferes with plant growth.

$LbFe^{II}NO$ has recently been detected by EPR spectroscopy also in intact nodules of soybean plants grown in the absence of nitrate [10]. Interestingly, significantly lower $LbFe^{II}NO$ concentrations were found in older nodules and essentially no $LbFe^{II}NO$ was present in senescent nodules [10]. In this work, we have shown that peroxynitrite oxidizes $LbFe^{II}NO$ to its iron(III) form ($LbFe^{II}NO$) rather efficiently. The second-order rate constant in the presence of physiologically relevant amounts of CO_2 (1 mM) is on the order of 10^5 M^{-1} s^{-1} (Table 1). Taken together, these observations suggest that senescent nodules exposed to an increased oxidative stress may have a lower $LbFe^{II}NO$ concentration because of its oxidation by peroxynitrite.

In conclusion, it appears that reactive nitrogen species are able to react with two inactive forms (in terms of oxygen binding) of Lb: ferrylLb and nitrosylLb. In both

cases, the product of the reactions is metLb, which has been detected in vivo [15]. As metLb can be reduced by a reductase found in the nodules [16], reactive nitrogen species could contribute to the recycling of these inactive forms to regenerate deoxyLb, the oxygen-binding form of Lb.

References

1. Davies MJ, Mathieu C, Puppo A (1999) Adv Inorg Chem 46:495–542
2. Ollis DL, Appleby CA, Colman PM, Cutten AE, Guss JM, Venkatappa MP, Freeman HC (1983) Aust J Chem 36:451–468
3. Hargrove MS, Barry JK, Brucker EA, Berry MB, Phillips GN Jr, Olson JS, Arredondo-Peter R, Dean JM, Klucas RV, Sarath G (1997) J Mol Biol 266:1032–1042
4. Gibson QH, Wittenberg JB, Wittenberg BA, Bogusz D, Appleby CA (1989) J Biol Chem 264:100–107
5. Moncada S, Palmer RMJ, Higgs EA (1991) Pharmacol Rev 43:109–142
6. Wendehenne D, Durner J, Klessig DF (2004) Curr Opin Plant Biol 7:449–455
7. Santos R, Hérouart D, Sigaud S, Touati D, Puppo A (2001) Mol Plant Microbe Interact 14:86–89
8. Hérouart D, Baudouin E, Frendo P, Harrison J, Santos R, Jamet A, Van de Sype G, Touati D, Puppo A (2002) Plant Physiol Biochem 40:619–624
9. Cueto M, Hernandez-Perera O, Martin R, Bentura ML, Rodrigo J, Lamas S, Golvano MP (1996) FEBS Lett 398:159–164
10. Mathieu C, Moreau S, Frendo P, Puppo A, Davies MJ (1998) Free Radical Biol Med 24:1242–1249
11. Maskall CS, Gibson JF, Dart PJ (1977) Biochem J 167:435–445
12. Nauser T, Koppenol WH (2002) J Phys Chem A 106:4084–4086
13. Radi R (2004) Proc Natl Acad Sci USA 101:4003–4008
14. Herold S, Puppo A (2005) J Biol Inorg Chem (this issue)
15. Lee K-K, Shearman LL, Erickson BK, Klucas RV (1995) Plant Physiol 109:261–267
16. Ji L, Becana M, Sarath G, Shearman L, Klucas RV (1994) Plant Physiol 106:203–209
17. Herold S, Röck G (2003) J Biol Chem 278:6623–6634
18. Koppenol WH, Kissner R, Beckman JS (1996) Methods Enzymol 269:296–302
19. Bohle DS, Glassbrenner PA, Hansert B (1996) Methods Enzymol 269:302–311
20. Herold S, Exner M, Boccini F (2003) Chem Res Toxicol 16:390–402
21. Harned HS, Bonner FT (1945) J Am Chem Soc 67:1026–1031
22. Puppo A, Rigaud J (1987) Electrophoresis 8:212–214
23. Aviram I, Wittenberg A, Wittenberg JB (1978) J Biol Chem 253:5685–5689
24. Herold S, Rehmann F-JK (2001) J Biol Inorg Chem 6:543–555
25. Herold S, Rehmann F-JK (2003) Free Radical Biol Med 34:531–545
26. Herold S, Exner M, Nauser T (2001) Biochemistry 40:3385–3395
27. Sharma VS, Traylor TG, Gardiner R, Mizukami H (1987) Biochemistry 26:3837–3843
28. Wanat A, Gdula-Argasinska J, Rutkowska-Zbik D, Witko M, Stochel G, van Eldik R (2002) J Biol Inorg Chem 7:165–176
29. Hoshino M, Maeda M, Konishi R, Seki H, Ford PC (1996) J Am Chem Soc 118:5702–5707
30. Herold S (2004) Inorg Chem 43:3783–3785
31. Hunt S, Gaito ST, Layzell DB (1988) Planta 173:128–141
32. Wiborg O, Hyldig-Nielsen JJ, Jensen EO, Paludan K, Marcker KA (1982) Nucl Acids Res 10:3487–3494
33. Lee HC, Wittenberg JB, Peisach J (1993) Biochemistry 32:11500–11506
34. Stetzkowski F, Cassoly R, Banejee R (1979) J Biol Chem 254:11351–11356
35. Mims MP, Porras AG, Olson JS, Noble RW, Peterson JA (1983) J Biol Chem 258:14219–14232
36. Laverman LE, Wanat A, Oszajca J, Stochel G, Ford PC, van Eldik R (2001) J Am Chem Soc 123:285–293
37. Cao W, Christian JF, Chiampion PM, Rosca F, Sage JT (2001) Biochemistry 40:5728–5737
38. Henderson RW, Appleby CA (1972) Biochim Biophys Acta 283:187–191
39. Puppo A, Monny C, Davies MJ (1993) Biochem J 289:435–438
40. Moreau S, Davies MJ, Mathieu C, Herouart D, Puppo A (1996) J Biol Chem 271:32557–32562
41. Davies MJ, Puppo A (1992) Biochem J 281:197–201
42. Moreau S, Davies MJ, Puppo A (1995) Biochim Biophys Acta 1251:17–22
43. Puppo A, Rigaud J, Job D (1981) Plant Sci Lett 22:353–360
44. Dalton DA, Post CJ, Langeberg L (1991) Plant Physiol 96:812–818
45. Giulivi C, Davies KJA (1990) J Biol Chem 265:19453–19460
46. Mathieu C, Swaraj K, Davies MJ, Trinchant J-C, Puppo A (1997) Free Rad Res 27:165–171
47. Dalton DA, Russell SA, Hanus FJ, Pascoe GA, Evans HJ (1986) Proc Natl Acad Sci USA 83:3811–3815
48. Moreau S, Puppo A, Davies MJ (1995) Phytochemistry 39:1281–1286
49. Exner M, Herold S (2000) Chem Res Toxicol 13:287–293
50. Boccini F, Herold S (2004) Biochemistry 43:16393–16404
51. Herold S (1999) FEBS Lett 443:81–84
52. Becana M, Sprent JI (1987) Physiol Plant 70:757–765
53. Kanayama Y, Yamamoto Y (1990) Plant Cell Physiol 31:603–608
54. Doyle M, Pickering R, DeWeert T, Hoekstra J, Pater D (1981) J Biol Chem 256:12393–12398
55. Kanayama Y, Watanabe I, Yamamoto Y (1990) Plant Cell Physiol 31:341–346
56. Gladwin MT, Crawford JH, Patel RP (2004) Free Radical Biol Med 36:707–717
57. Yamasaki H, Sakihama Y, Takahashi S (1999) Trends Plant Sci 4:128–129
58. Desikan R, Griffiths R, Hancock J, Neill S (2002) Proc Natl Acad Sci USA 99:16314–16318
59. Meyer C, Lea US, Provan F, Kaiser WM, Lillo C (2005) Photosynth Res 83:181–189
60. Addison AW, Stephanos JJ (1986) Biochemistry 25:4104–4113
61. Antonini E, Brunori M (1971) Hemoglobin and myoglobin in their reactions with ligands. North-Holland, Amsterdam